Supporting Information

Cobalt nanoparticles encapsulated in carbon nanotube-grafted nitrogen and sulfur co-doped multichannel carbon fibers as efficient bifunctional oxygen electrocatalysts

Zhe Wang,[a,b] Shengjie Peng,*[b, c] Yuxiang Hu,[d] Linlin Li,[c,e] Tao Yan,[a] Guorui Yang,[b] Dongxiao Ji,[b] Srinivasan Madhavi,[e] Zhijuan Pan, *[a] and Seeram Ramakrishna[b]

Table S1 Detail preparation information of different samples.

Sample	Precursor solution	Stabilization	Carbonization	Further (second) pyrolusis
MCF-900	PAN, and PS in DMF	280 °C for 2 h in air	700 °C for 3 h under H_2/Ar atmosphere	900 °C for 2 h under N_2 atmosphere
NS/MCF-900	PAN, PS, and TAA in DMF	280 °C for 2 h in air	700 °C for 3 h under H_2/Ar atmosphere	900 °C for 2 h under N_2 atmosphere
Co@NS/MCF-900	PAN, PS, TAA, and cobalt(III) acetylacetonate in DMF	280 °C for 2 h in air	700 °C for 3 h under H_2/Ar atmosphere	900 °C for 2 h under N_2 atmosphere
Co@NS/CNTs-MCF-700	PAN, PS, TAA, and cobalt(III) acetylacetonate in DMF	280 °C for 2 h in air	700 °C for 3 h under H_2/Ar atmosphere	With melamine 700 °C for 2 h under N_2 atmosphere
Co@NS/CNTs-MCF-800	PAN, PS, TAA, and cobalt(III) acetylacetonate in DMF	280 °C for 2 h in air	700 °C for 3 h under H_2/Ar atmosphere	With melamine 800 °C for 2 h under N_2 atmosphere
Co@NS/CNTs-MCF-900	PAN, PS, TAA, and cobalt(III) acetylacetonate in DMF	280 °C for 2 h in air	700 °C for 3 h under H_2/Ar atmosphere	With melamine 900 °C for 2 h under N_2 atmosphere
Co@NS/CNTs-MCF-1000	PAN, PS, TAA, and cobalt(III) acetylacetonate in DMF	280 °C for 2 h in air	700 °C for 3 h under H_2/Ar atmosphere	With melamine 1000 °C for 2 h under N_2 atmosphere

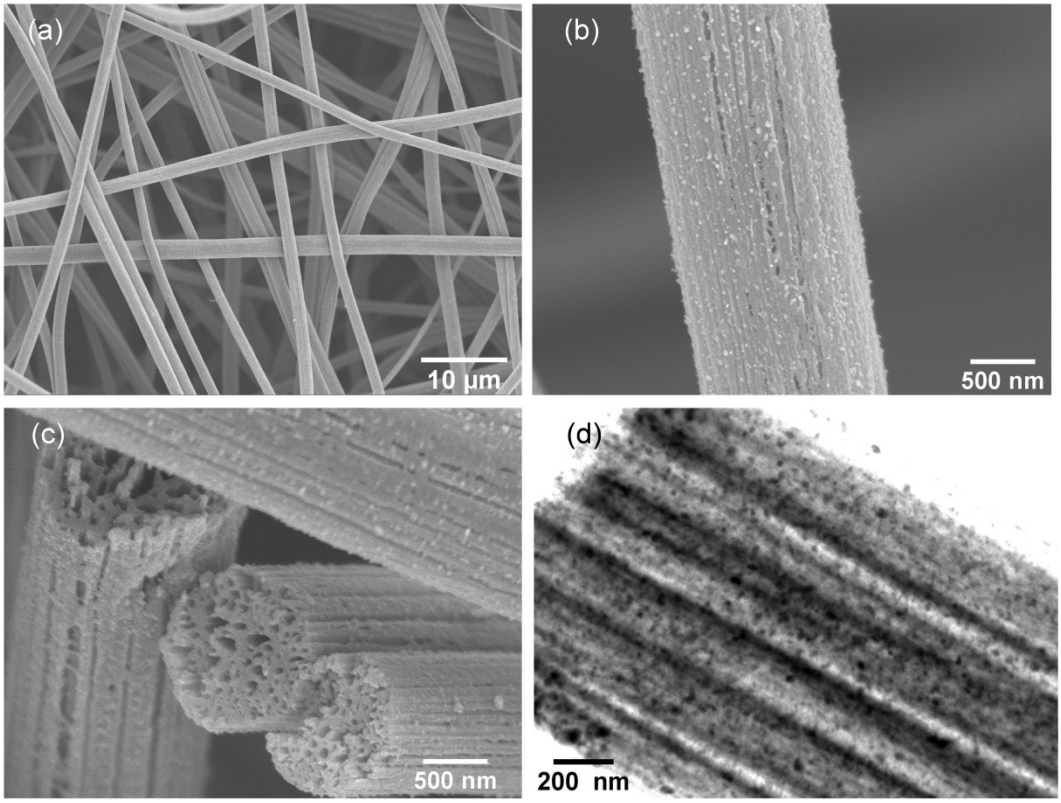

Fig. S1 Morphology and structural characterization of Co@NS/MCF obtained at 700 °C in H_2/Ar atmosphere for 3 h. a, b) SEM images; c) the corresponding cross-sectional image and d) the TEM image.

The SEM and TEM images show the multichannel structure of Co@NS/MCF with the Co NPs uniformly dispersed.

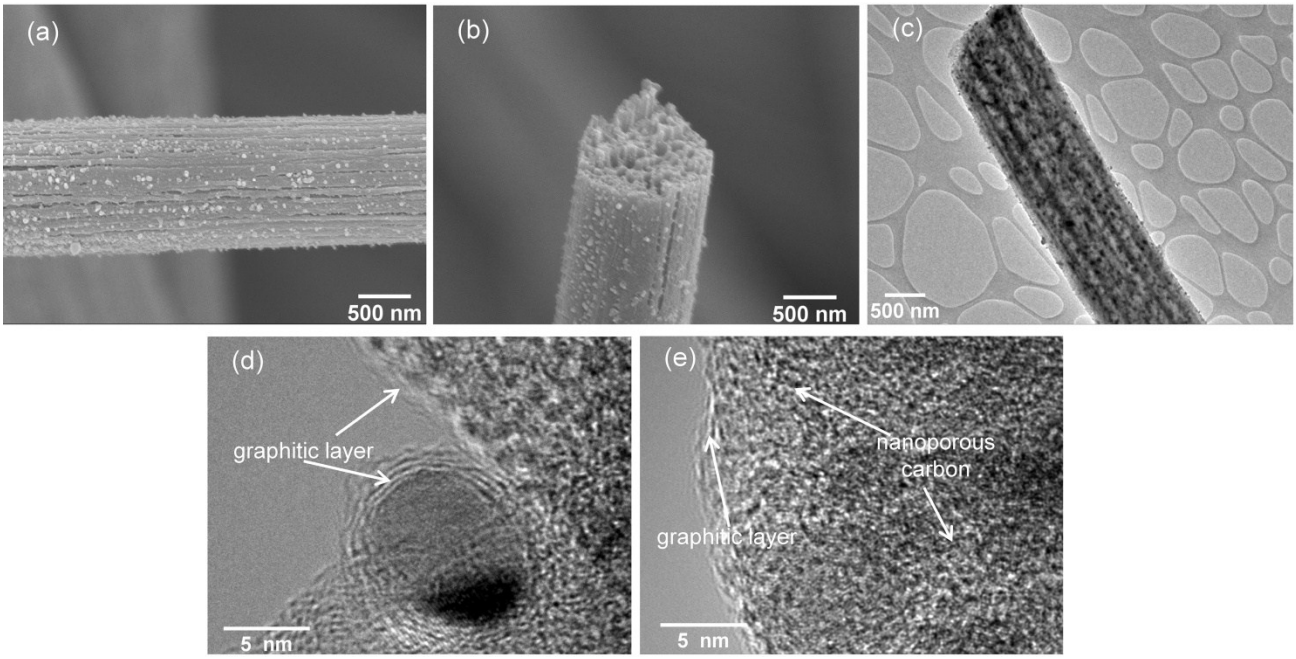

Fig. S2 a, b) SEM images of Co@NS/MCF-900 carbon fiber; c) the corresponding TEM image; d, e) HRTEM images of Co NPs and carbon nanostructure on Co@NSMCF-900, respectively.

Fig. S2a, b, and c show the multichannel structure of Co@NS/MCF-900 with the Co NPs uniformly dispersed. Fig. S2d reveals that Co NP was coated by few graphitic carbon layers. Fig. S2e shows the multichannel fiber is of highly porous with few graphitic layers.

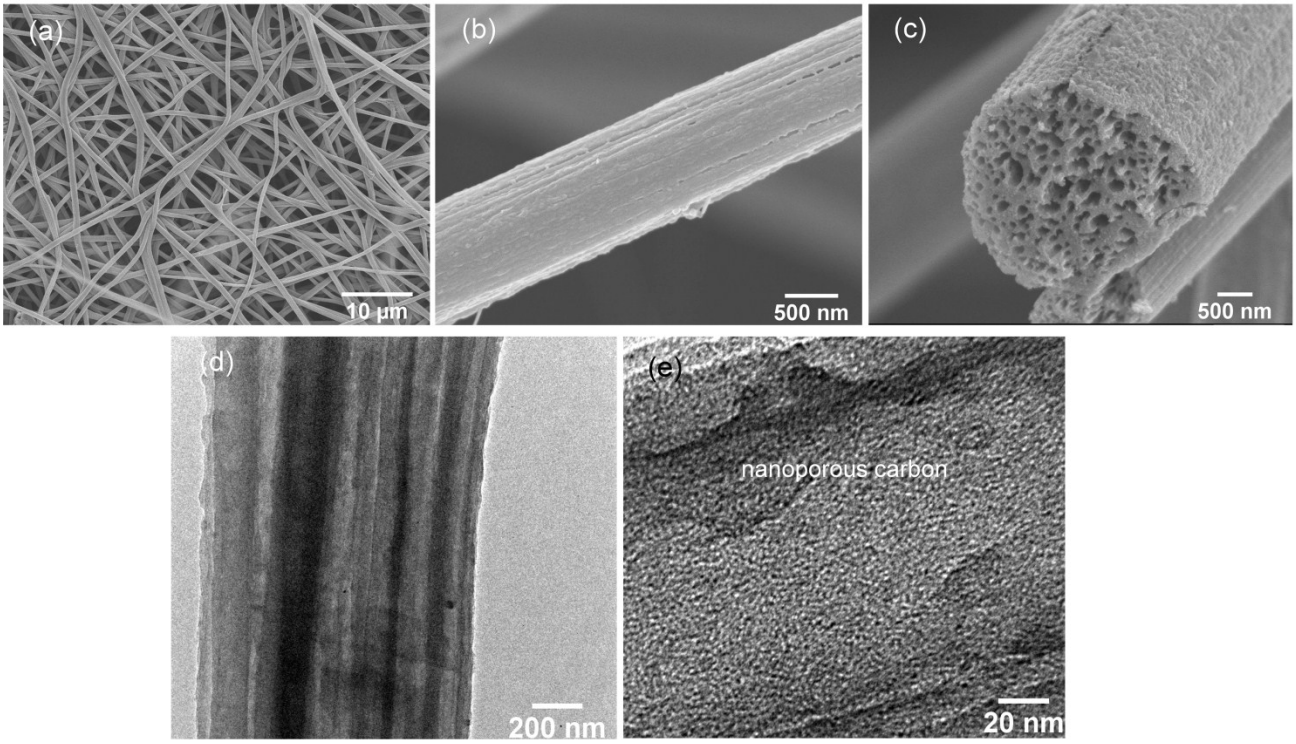

Fig. S3 a, b, and c) SEM images of NS/MCF-900 carbon fiber; d) the corresponding TEM image; e) HRTEM image of carbon nanostructure on NS/MCF-900

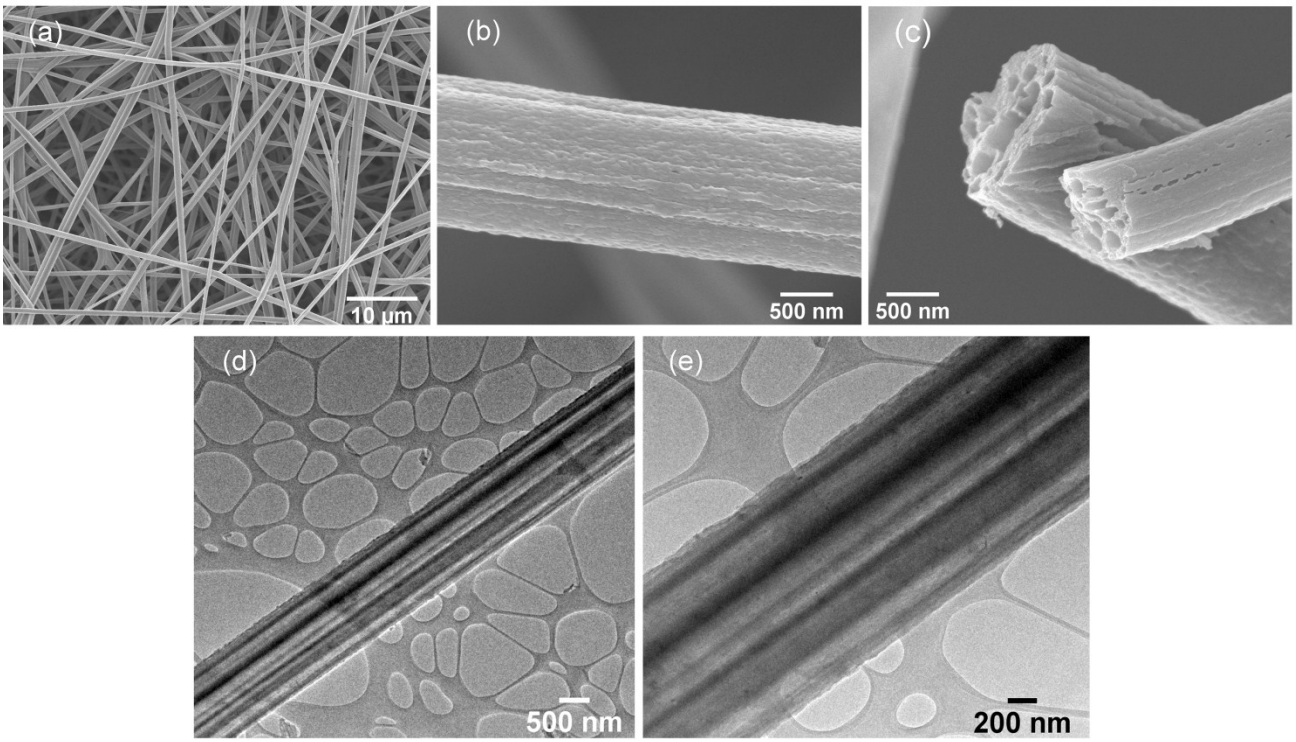

Fig. S4 a, b, and c) SEM images of MCF-900 carbon fiber; d, e) the corresponding TEM images.

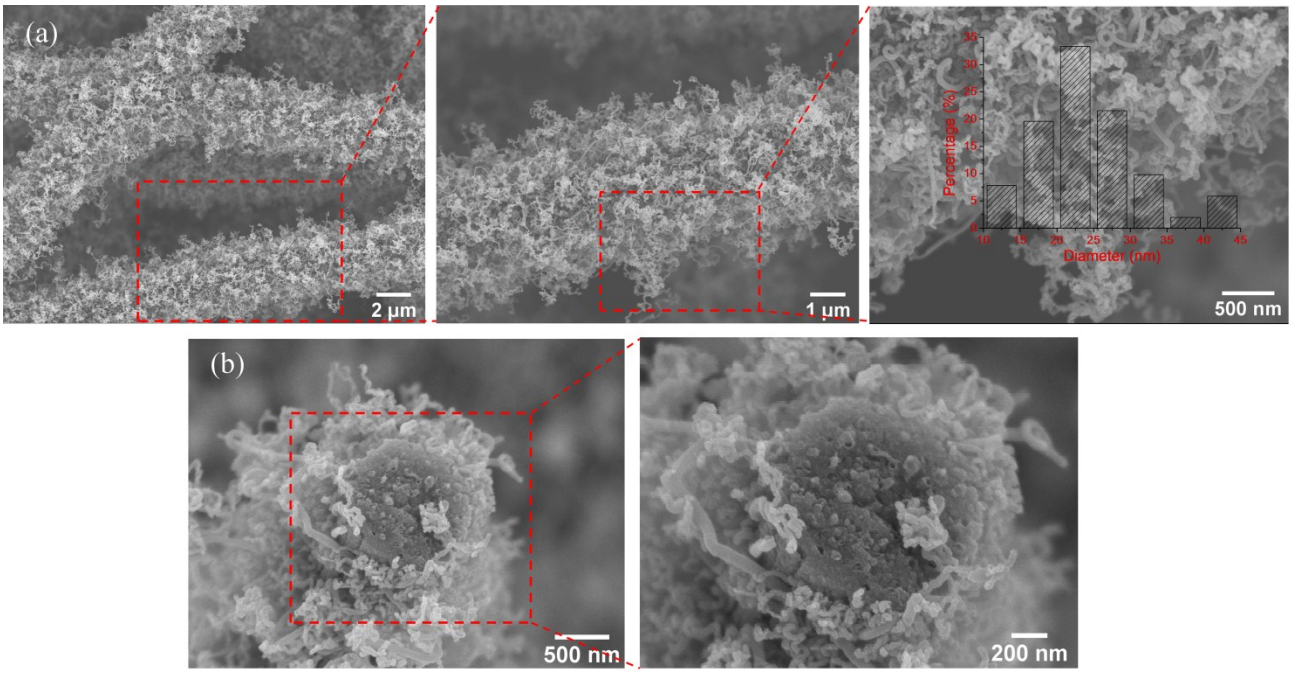

Fig. S5 a) SEM images of Co@NS/CNTs-MCF-900, and the inset shows the diameter distribution of CNTs; b) the corresponding cross-sectional image.

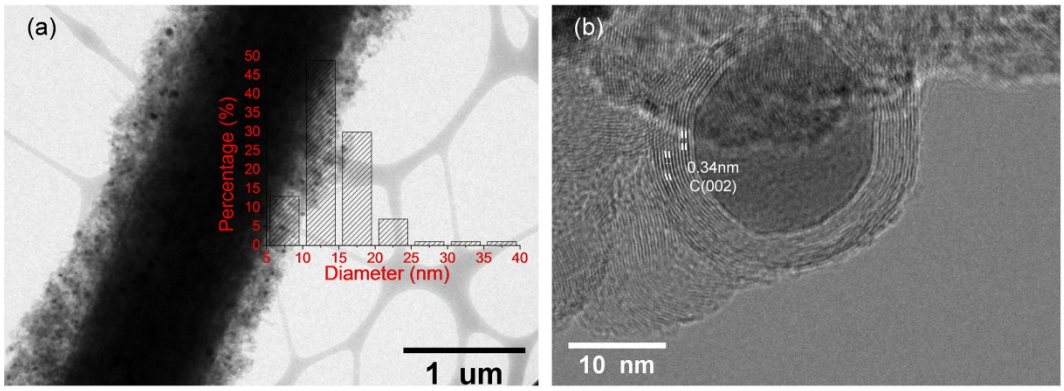

Fig. S6 a) TEM image of Co@NS/CNTs-MCF-900 carbon fiber, and the inset shows the diameter distribution of Co NPs; b) HRTEM of Co NPs coated by several graphitic layers.

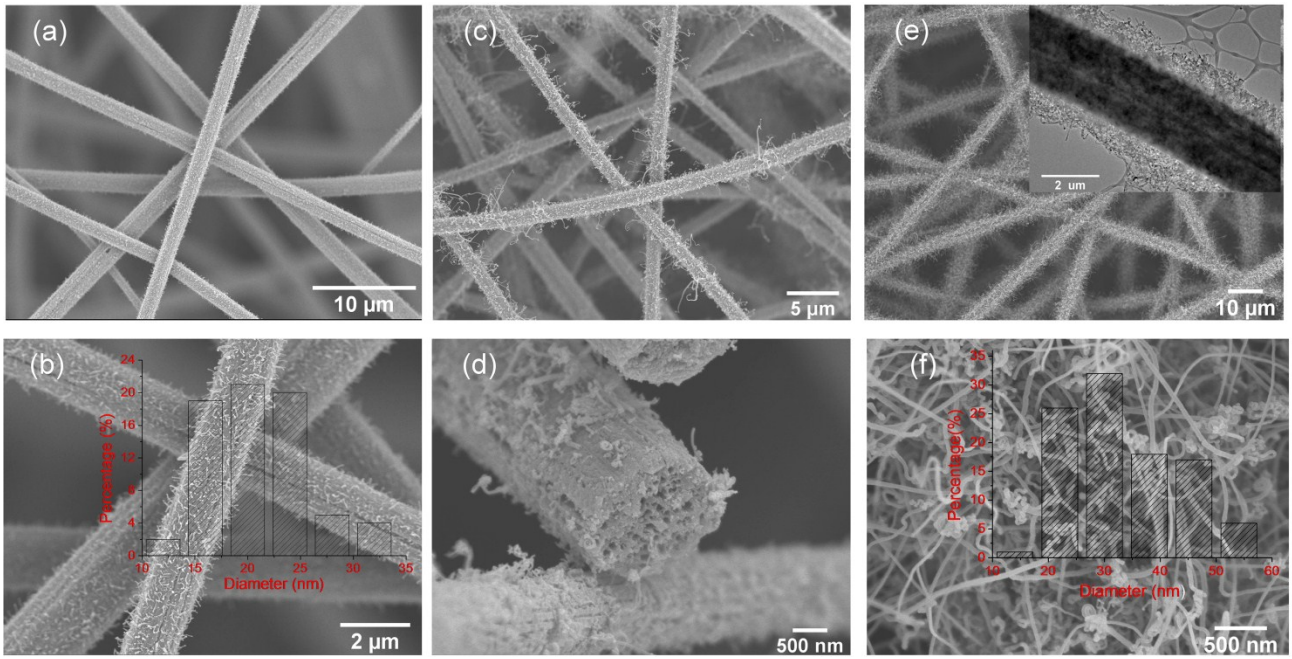

Fig. S7 a,b) SEM images of Co@NS/CNTs-MCF-700 carbon fibers and the inset shows the diameter distribution of CNTs; c) SEM image of Co@NS/CNTs-MCF-800 carbon fibers and d) the corresponding cross-sectional image; e) SEM image of Co@NS/CNTs-MCF-1000 carbon fibers, and the inset shows the corresponding TEM image; f) SEM of CNTs grafted on Co@NS/CNTs-MCF-1000 and the inset shows the diameter distribution of CNTs.

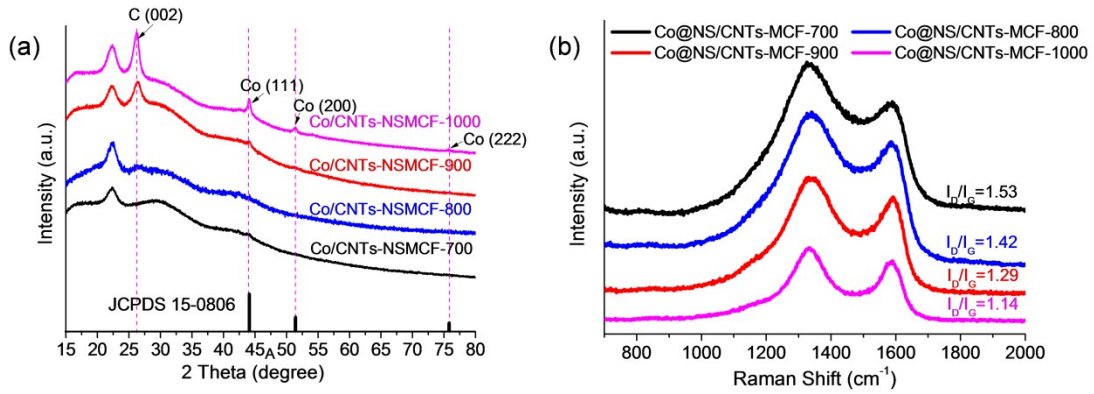

Fig. S8 a) XRD patterns and b) Raman spectra of Co@NS/CNTs-MCF-700, Co@NS/CNTs-MCF-800, Co@NS/CNTs-MCF-900, and Co@NS/CNTs-MCF-1000, respectively

Table S2 Atomic contents of Co@NS/CNTs-MCF-700, Co@NS/CNTs-MCF-800, Co@NS/CNTs-MCF-900, and Co@NS/CNTs-MCF-1000, calculated form the XPS survey spectra

Sample	C (at. %)	Co (at. %)	N (at. %)	S (at. %)	O (at. %)
Co@NS/CNTs-MCF-700	84.29	2.05	9.29	0.40	3.97
Co@NS/CNTs-MCF-800	87.44	1.53	8.41	0.28	2.35
Co@NS/CNTs-MCF-900	91.68	0.60	6.54	0.12	1.06
Co@NS/CNTs-MCF-1000	94.49	0.32	2.87	0	0.49

Table S3 Cobalt content in Co@NS/CNTs-MCF-700, Co@NS/CNTs-MCF-800, Co@NS/CNTs-MCF-900, and Co@NS/CNTs-MCF-1000, determined by ICP-AES

Sample	Co@NS/CNTs-MCF-700	Co@NS/CNTs-MCF-800	Co@NS/CNTs-MCF-900	Co@NS/CNTs-MCF-1000
Co (wt %)	10.21	7.23	3.57	2.46

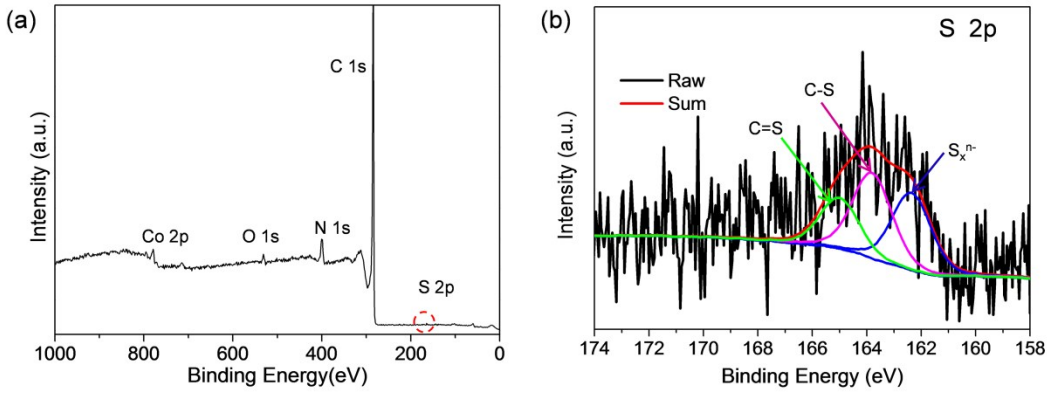

Fig. S9 a) XPS survey scan of Co@NS/CNTs-MCF-900; b) high-resolution and the corresponding deconvoluted S 2p spectra of Co@NS/CNTs-MCF-900.

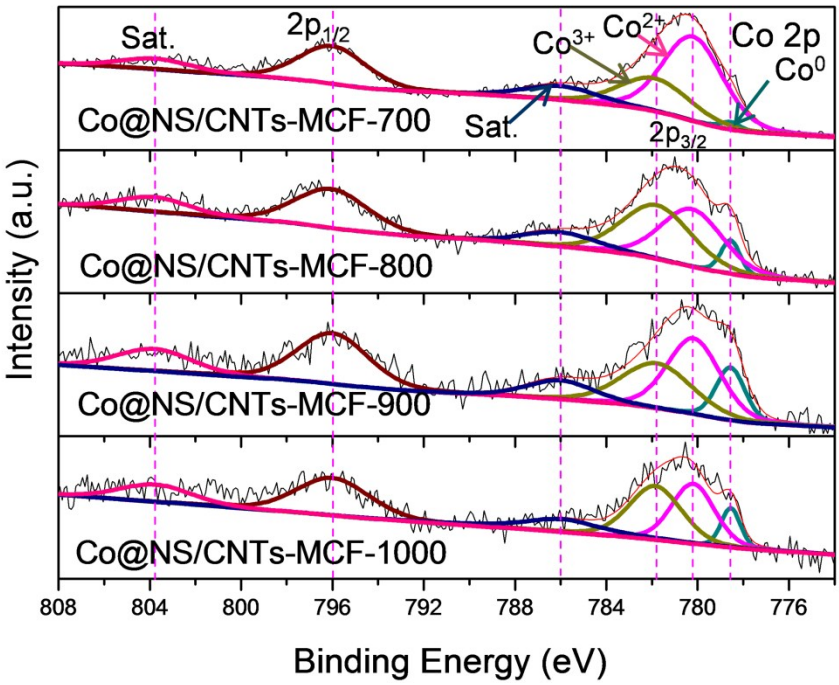

Fig. S10 High-resolution and the corresponding deconvoluted Co 2p XPS spectrum of Co@NS/CNTs-MCF-700, Co@NS/CNTs-MCF-800, Co@NS/CNTs-MCF-900, and Co@NS/CNTs-MCF-1000, respectively.

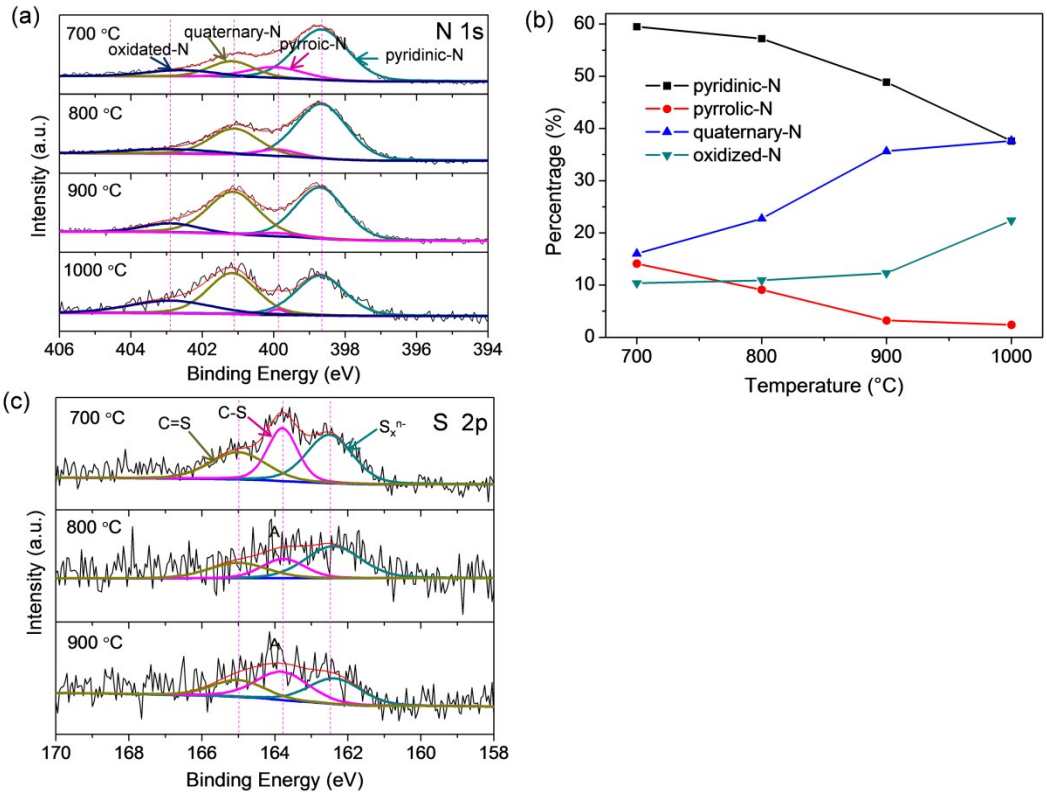

Fig. S11 a) high-resolution and the corresponding deconvoluted N 1s XPS spectrum of Co@NS/CNTs-MCF-700, Co@NS/CNTs-MCF-800, Co@NS/CNTs-MCF-900, and Co@NS/CNTs-MCF-1000; b) the corresponding contents of pyridinic-N, pyrrolic-N, graphitic-N, and oxidated-N; c) high-resolution and the corresponding deconvoluted S 2p XPS spectra of Co@NS/CNTs-MCF-700, Co@NS/CNTs-MCF-800, and Co@NS/CNTs-MCF-900.

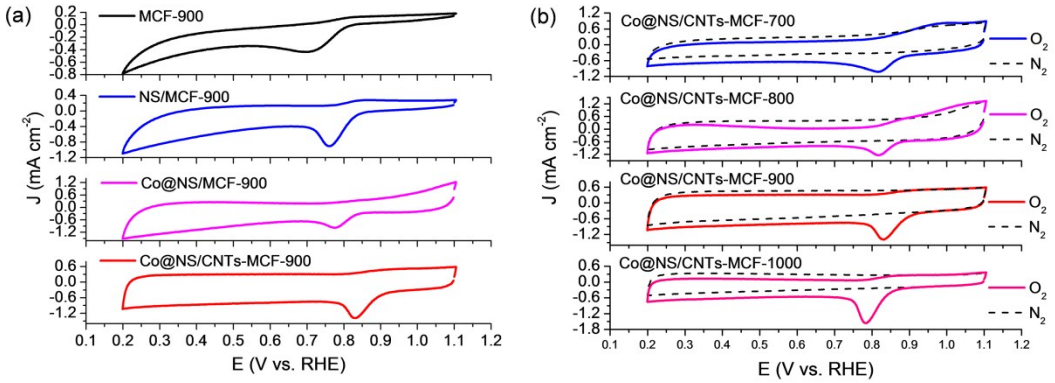

Fig. S12 a) CV curves of MCF-900, NS/MCF-900, Co@NS/MCF-900, and Co@NS/CNTs-MCF-900 at a scan rate of 50 mV s^{-1} in O_2-saturated 0.1 M KOH; b) CV curves of Co@NS/CNTs-MCF-700, Co@NS/CNTs-MCF-800, Co@NS/CNTs-MCF-900, and Co@NS/CNTs-MCF-1000 at a scan rate of 50 mV s^{-1} in N_2 and O_2-saturated 0.1 M KOH, respectively.

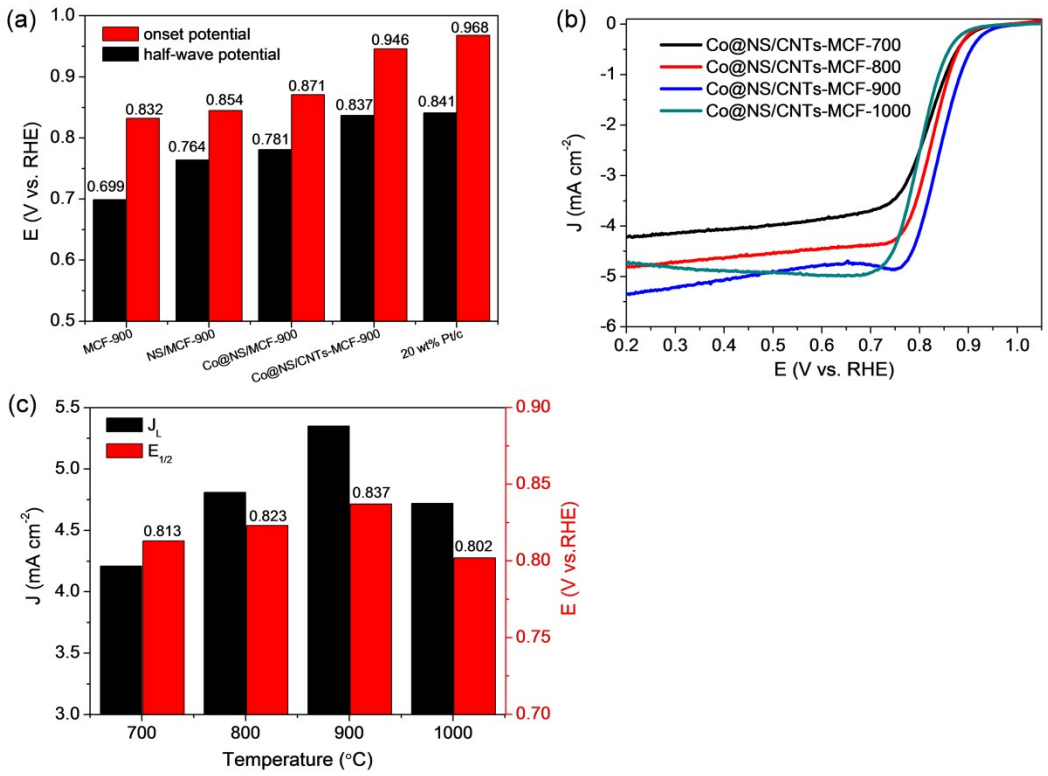

Fig. S13 a) onset potentials and half-wave potentials of MCF-900, NS/MCF-900, Co@NS/MCF-900, and Co@NS/CNTs-MCF-900, respectively; b) LSV curves of Co@NS/CNTs-MCF-700, Co@NS/CNTs-MCF-800, Co@NS/CNTs-MCF-900, and Co@NS/CNTs-MCF-1000 at 5 mV s^{-1} and a rotation speed of 1600 rpm; c) the corresponding diffusion-limited current densities at 0.20 V (vs. RHE) and half-wave potentials.

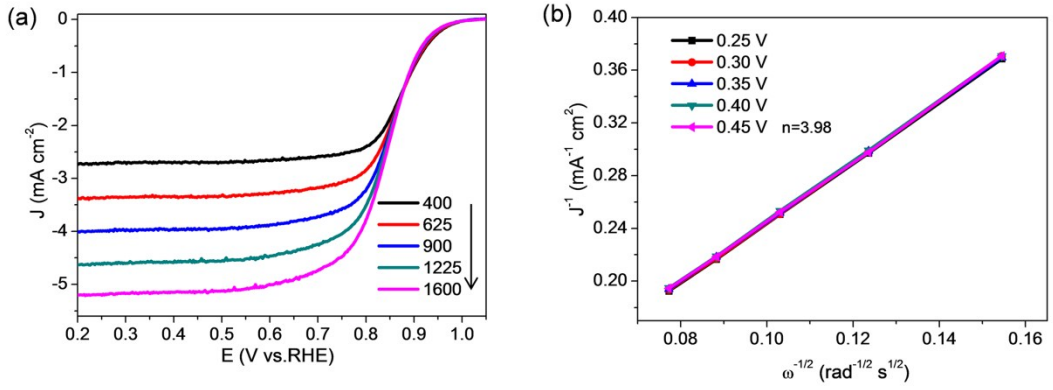

Fig. S14 a) LSV curves of commercial 20 wt% Pt/C catalyst in O_2-saturated 0.1 M KOH at various rotation speeds; b) the corresponding K-L plots at different potentials.

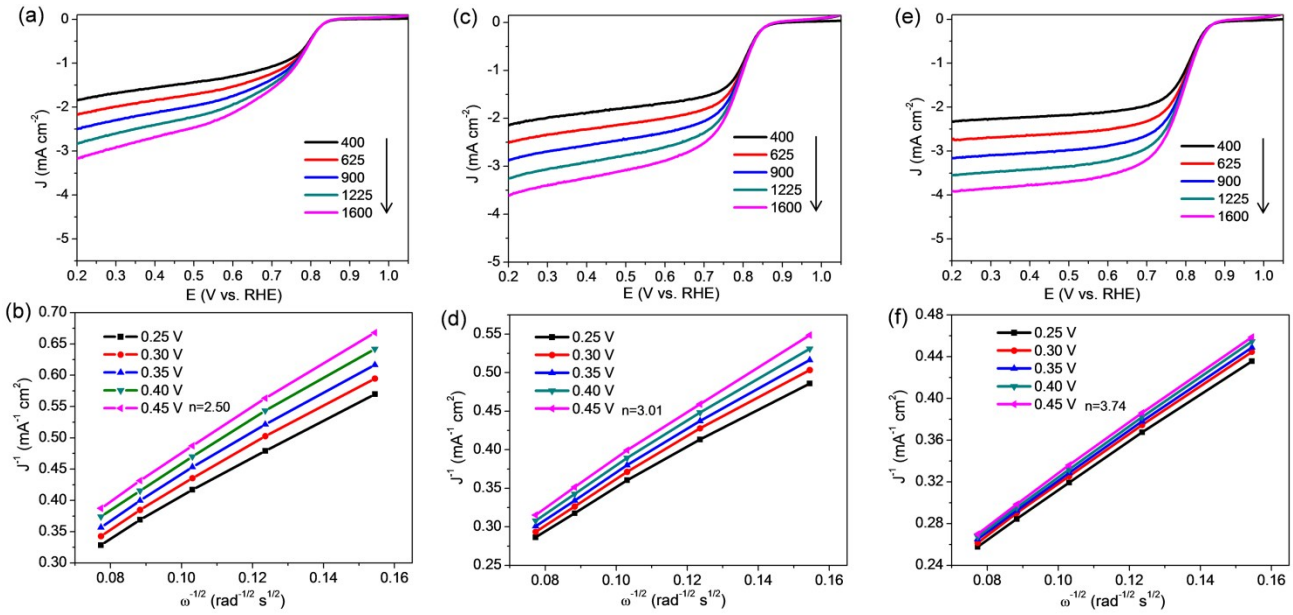

Fig. S15 a, c, e) LSV curves of MCF-900, NS/MCF-900, and Co@NS/-MCF-900 in O_2-saturated 0.1 M KOH at various rotation speeds, respectively; b, d, f) the corresponding K-L plots at different potentials.

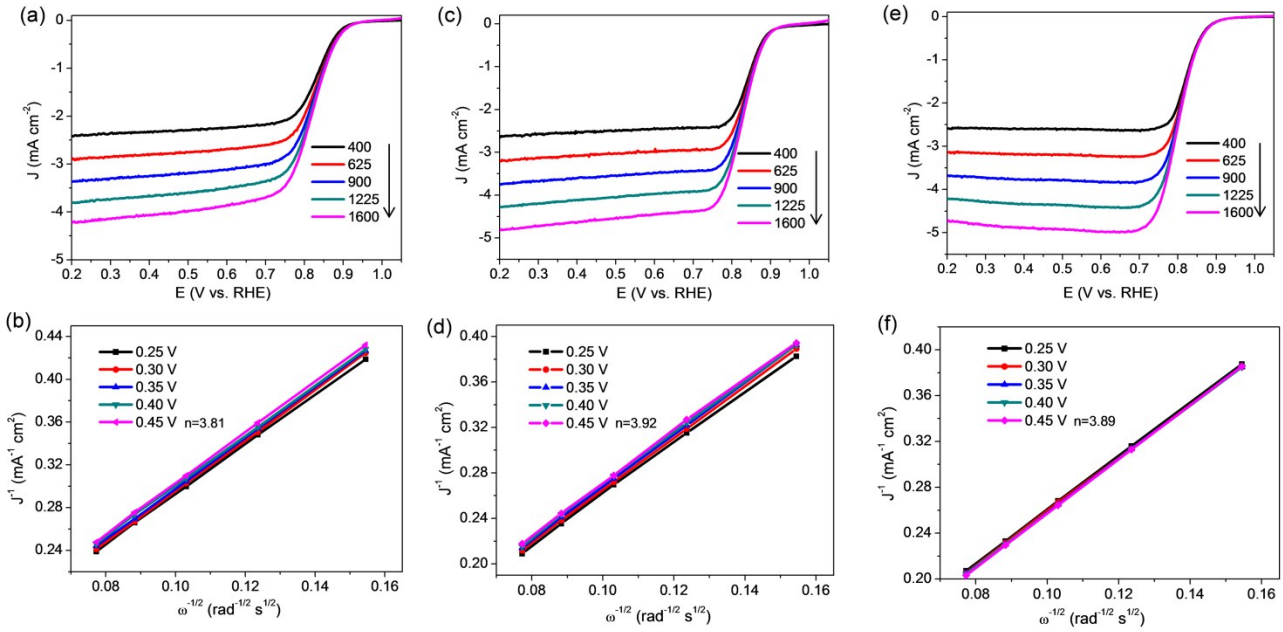

Fig. S16 a, c, e) LSV curves of Co@NS/CNTs-MCF-700, Co@NS/CNTs-MCF-800 , and Co@NS/CNTs-MCF-1000 in O_2-saturated 0.1 M KOH at various rotation speeds, respectively; b, d, f) the corresponding K-L plots at different potentials

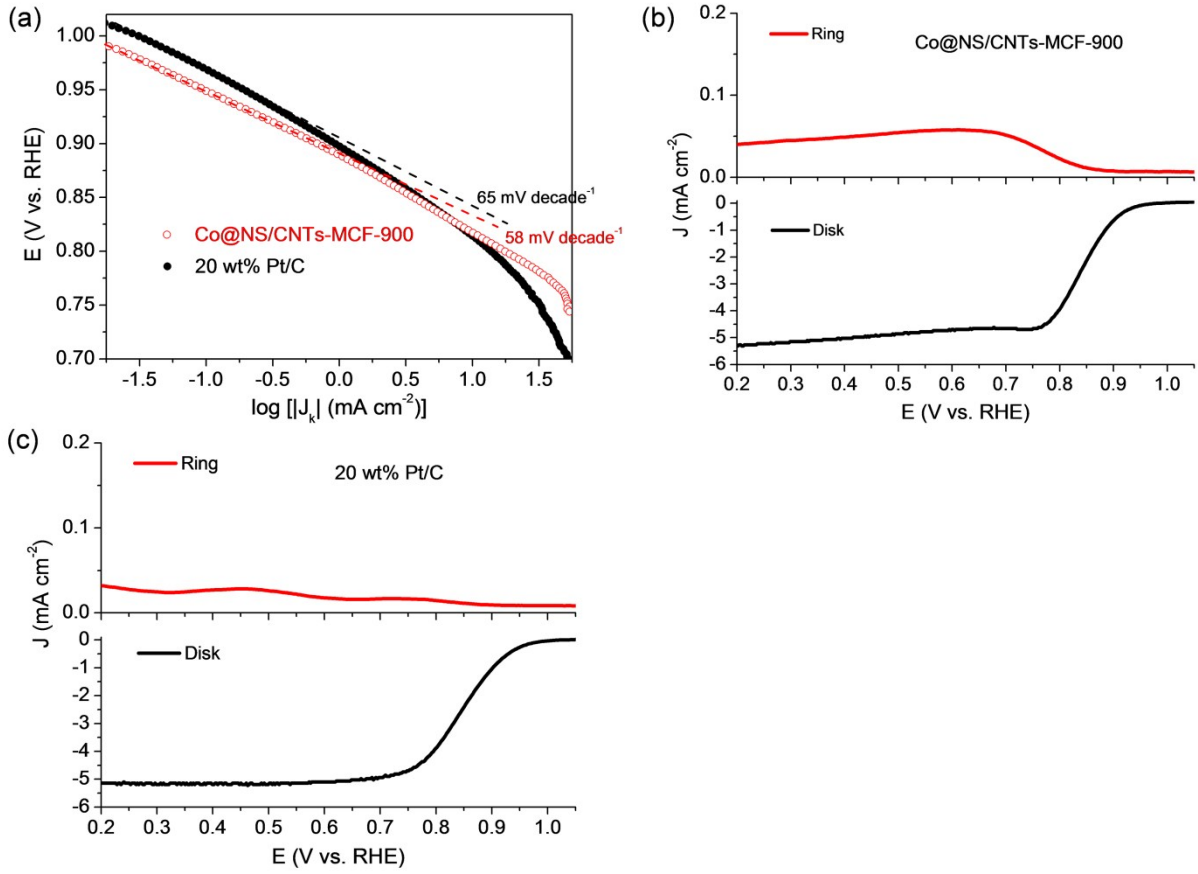

Fig. S17 a) Tafel plots of Co@NS/CNTs-MCF-900 and commercial 20 wt% Pt/C catalyst; b) RRDE results of Co@NS/CNTs-MCF-900; c) RRDE results of commercial 20 wt% Pt/C catalyst.

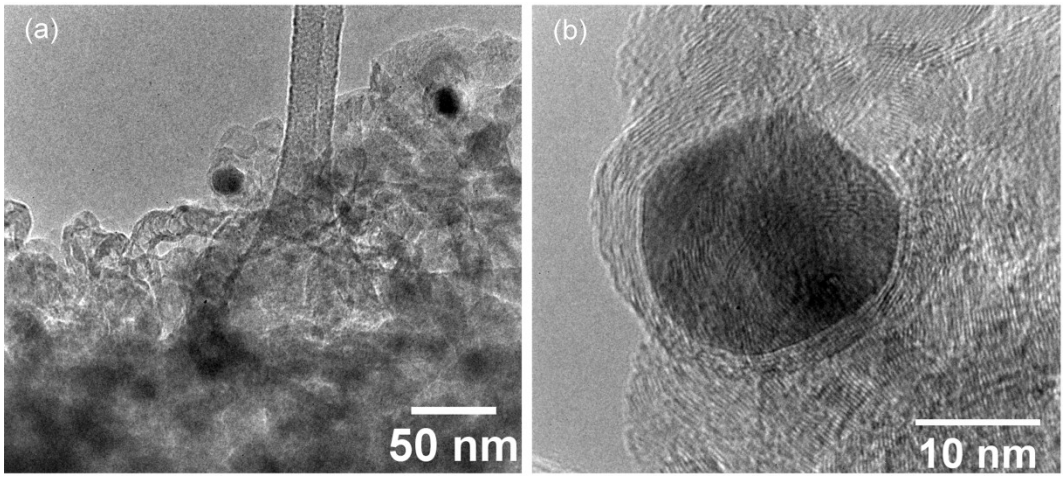

Figure S18. (a) TEM and (b) HRTEM of Co NPs coated by several graphitic shells after ORR durability test for about 24 h.

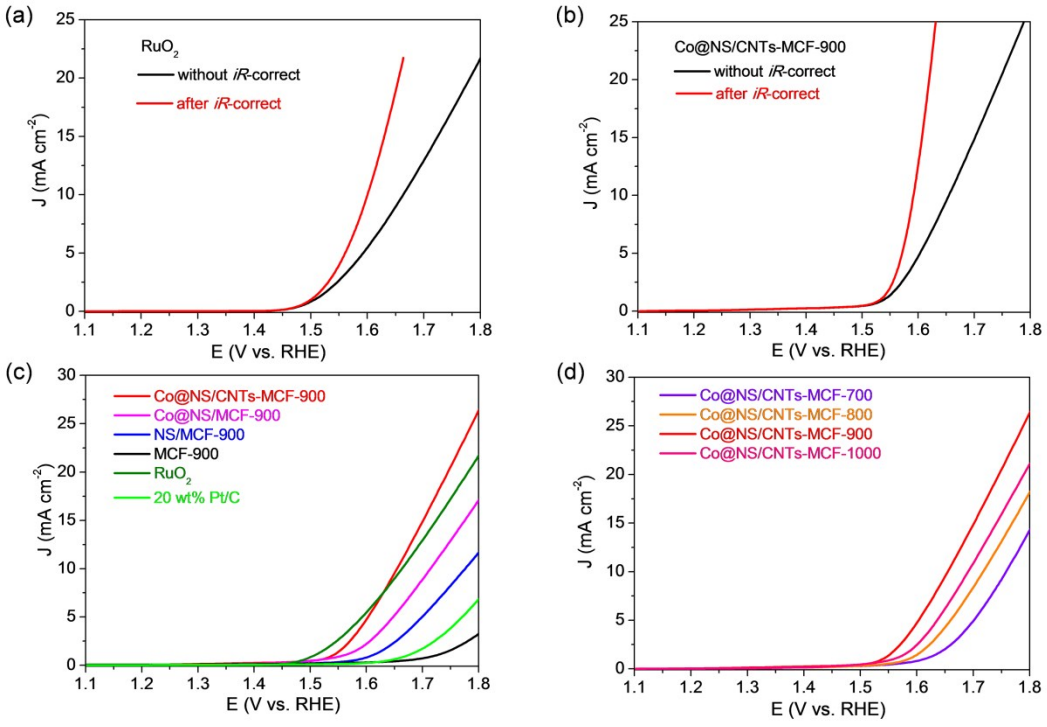

Fig. S19 a) Polarization curves of commercial RuO_2 catalyst with (red) and without (black) iR-correct at a scan rate of 5 mV s^{-1} and 1600 rpm in O_2-saturated 0.1 M KOH solution; b) polarization curves of Co@NSCNTs-MCF-900 with (red) and without (black) iR-correct; c) polarization curves of MCF-900, NS/MCF-900, Co@NS/MCF-900, Co@NS/CNTs-MCF-900, commercial RuO_2, and 20 wt% Pt/C catalysts without iR correct; d) polarization curves of

Co@NS/CNTs-MCF-700, Co@NS/CNTs-MCF-800, Co@NS/CNTs-MCF-1000, without iR correct. The solution resistance was determined by the EIS technique.

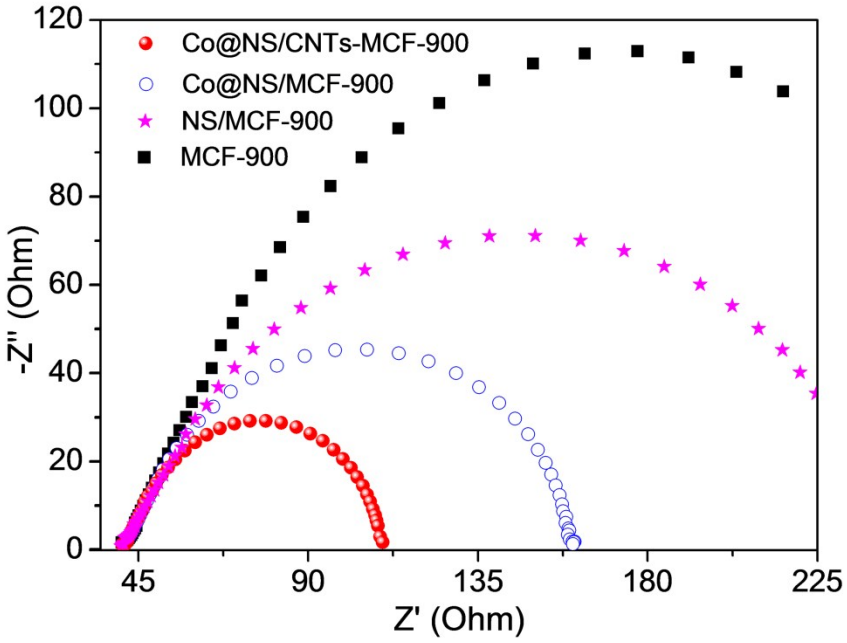

Fig. S20 The electrochemical impedance spectroscopy (EIS) spectra of MCF-900, NS/MCF-900, Co@NS/MCF-900, and Co@NS/CNTs-MCF-900, measured within the frequency range from 0.01 to 100 kHz at 1.65 V (vs. RHE) and a potentiostatic signal amplitude of 5 mV in 0.1 M KOH.

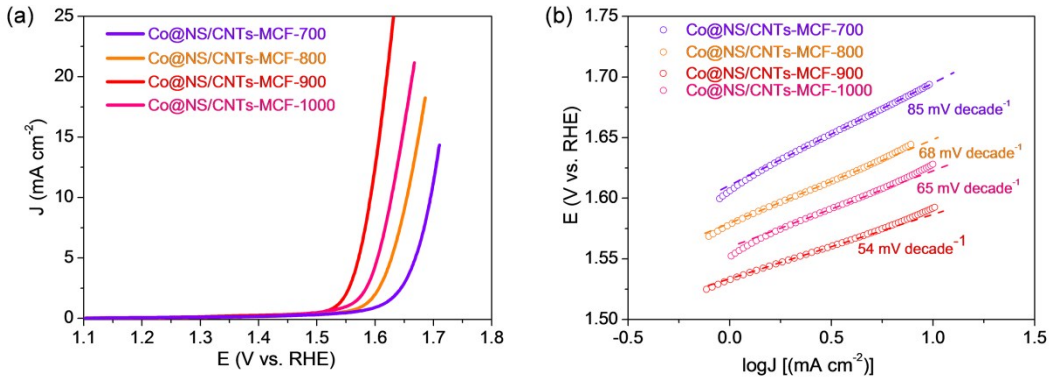

Fig. S21 a) iR-corrected polarization curves for OER at a scan rate of 5 mV s^{-1} and 1600 rpm in O_2-saturated 0.1 M KOH solution on Co@NS/CNTs-MCF-700, Co@NS/CNTs-MCF-800, Co@NS/CNTs-MCF-900, and Co@NS/CNTs-MCF-1000; b) the corresponding Tafel plots.

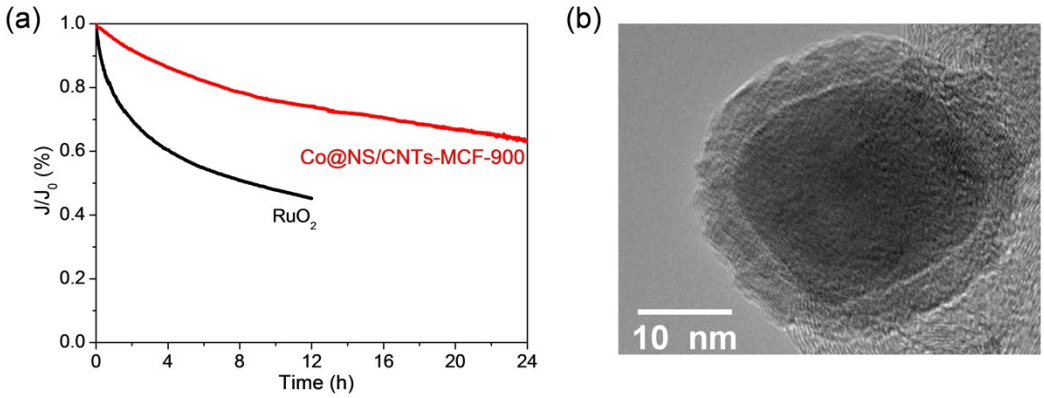

Fig. S22 (a) Current-time chronoamperometric responses of Co@NS/CNTs-MCF-900 and commercial RuO2 catalyst at a constant voltage of 1.60 V (vs. RHE) in O2-saturated 0.1 M KOH; (b) HRTEM of Co NPs coated by several graphitic shells after OER durability test for about 24 h.

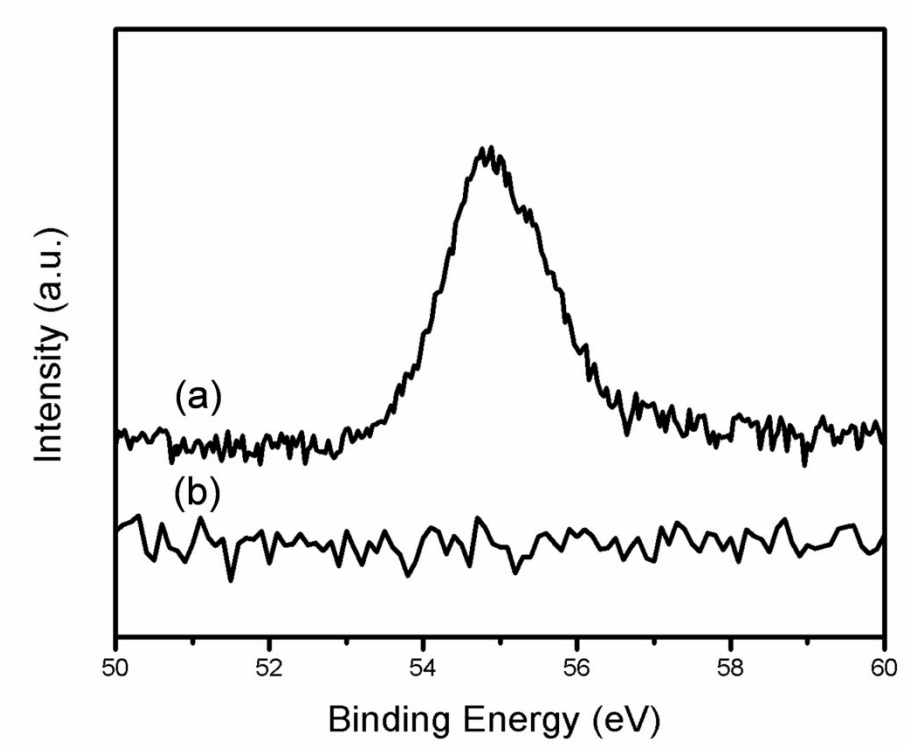

Fig. S23 Li 1s XPS spectra of the a) discharged and b) charged Co@NS/CNTs-MCF-900 mat cathode.

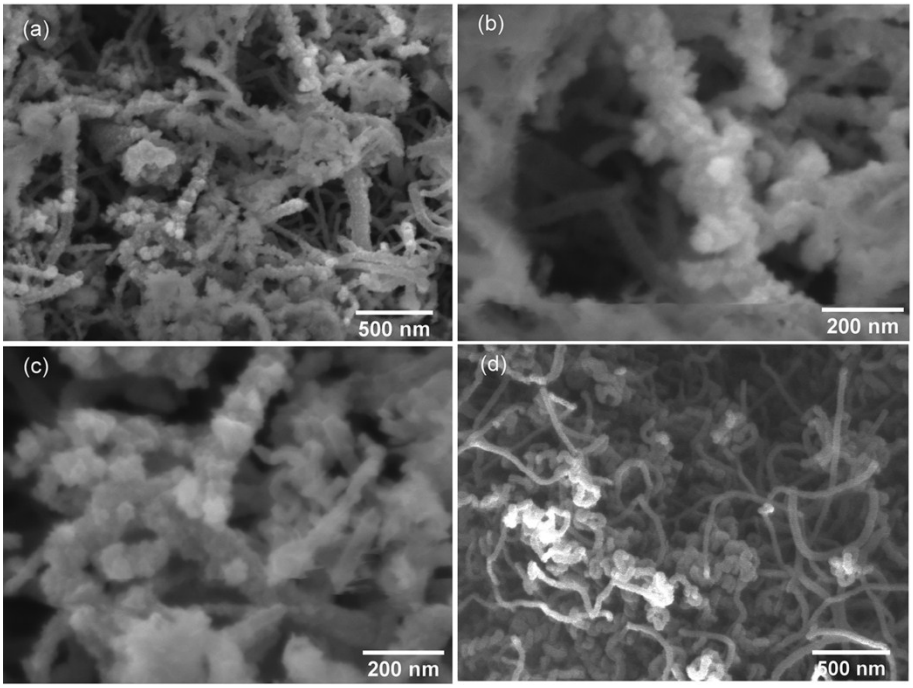

Fig. S24 a) SEM image of discharged Co@NS/CNTs-MCF-900 mat cathode; b,c) the corresponding high-magnified SEM images; d) SEM image of charged Co@NS/CNTs-MCF-900 mat cathode.

Table S4 Comparison of the ORR performance of different catalysts.

Catalyst	CatalystLoading (mg cm^{-2})	Onset potential (V vs. RHE)	Half-wave potential (Vvs. RHE)	n	Electrolyte	Supplementary Reference
Co@NS/CNTs-MCF-900	0.6	0.946	0.837	3.97	0.1 M KOH	This work
Co_3O_4/N-rmGO	0.17	0.88	0.83	3.9	0.1 M KOH	1
Fe-N-CNFs	0.60	0.93	0.81	3.93	0.1 M KOH	2
Co_9S_8@CNS 900	0.4	0.927	0.807	3.97	0.1 M KOH	3
Co_3O_4/NPGC	0.2	0.97	0.842	~4	0.1 M KOH	4
N/Co-doped PCP//NRGO	0.714	0.97	0.86	3.90-3.94	0.1 M KOH	5
N-carbon nanotube frameworks	0.2	0.97	0.87	3.97	0.1 M KOH	6
Fe-N-CC	0.1	0.94	0.83	~3.8	0.1 M KOH	7
Fe-N/C-800	0.1	0.923	0.809	4.15	0.1 M KOH	8
P-CNCo-20	0.1	0.93	0.85	3.9	0.1 M KOH	9
Co@Co_3O_4@C-CM	0.1	0.93	0.81	3.8	0.1 M KOH	10
LDG@ZIF-CoZn-800	0.2	0.976	0.849	3.96	0.1 M KOH	11
CoP-CMP800	0.6	0.88	0.82	3.83-3.86	0.1 M KOH	12
Co,N-CNF	0.12	-0.082 (vs Ag/AgCl)	-0.155 (vs Ag/AgCl)	N/A	0.1 M KOH	13
Pt/C	0.1	0.9	0.841	3.98	0.1 M KOH	This work

Table S5 Comparison of the OER performance of different catalysts.

Catalyst	Catalyst Loading (mg cm^{-2})	Overpotential η (m V) @ 10 mA cm^{-2}	Tafel slop (mV dec^{-1})	Electrolyte	Supplementary Reference
Co@NS/CNTs-MCF-900	0.6	357 mV	54	0.1 M KOH	This work
Co_3O_4/N-rmGO	1	310 mV	67	1 M KOH	1
N-CG-CoO	0.71	340 mV	71	1 M KOH	14
CoNP@NC/NG-700	N/A	390 mV	78	0.1 M KOH	15
SC CoO NRs	0.40	330 mV	44	1 M KOH	16
Co-P film	1	345 mV	47	1 M KOH	17
CoP NR/C	0.71	320 mV	71	1 M KOH	18
NiCo LDH	N/A	367 mV	40	1 M KOH	19
Co_xO_y/NC	0.21	430 mV	74.8	0.1 M KOH	20
NG-$CoSe_2$ composite	0.2	366 mV	40	0.1 M KOH	21
Co/N-C-800	0.25	371 mV	61.4	0.1 M KOH	22
Ni-Co_2-O	0.2	362 mV	64.4	0.1 MKOH	23
Annealed C-Co	0.2	390	N/A	0.1 MKOH	24
Co_2B-500	0.21	380	45	0.1 MKOH	25
Mn_3O_4/$CoSe_2$	0.2	450	49	0.1 MKOH	26
N-Co_9S_8/G	0.2	409 mV	82.7	0.1 M KOH	27
RuO_2	0.2	360 mV	58	0.1 M KOH	This work

Table S6 Comparison of the highly active ORR-OER activities of different catalysts.

Catalyst	Catalyst Loading (mg cm^{-2})	$E_{1/2}$ (V) ORR Half-wave potential	$E_{J=10}$ (V) OER@ 10 mA cm^{-2}	Overall oxygen activity $\Delta E=E_{J=10}-E_{1/2}$	Electrolyte	Supplementary Reference
Co@NS/CNTs-MCF-900	0.6	0.837	1.592	0.755	0.1 M KOH	This work
Co_3O_4/N-rmGO	1	0.86	1.54	0.71	1 M KOH	1
NCNTFs	0.2	0.87	1.60	0.73	0.1 M KOH	6
N-CG-CoO	0.7	0.81	1.57	0.76	1 M KOH	14
SC CoO NRs	0.4	0.85	1.56	0.71	1 M KOH	16
Co@Co_3O_4/NC-1	0.21	0.80	1.65	0.86	0.1 M KOH	28
NCT/$Co_xMn_{1-x}O$	0.21	0.84	1.57	0.73	1 M KOH	29
Co/N-CNTs	0.20	0.84	1.62	0.78	0.1 M KOH	30
N-GRW	0.6	0.84	1.59	0.75	1 M KOH	31
Co_3O_4/NBGFSs	0.13	0.862	1.70	0.838	0.1 M KOH	32
CoS_2(400)/N,S-Go	0.25	0.79	1.61	0.82	0.1 M KOH	33
Co_3O_4C-NA	0.2	0.78	1.52	0.74	0.1 M KOH	34

Supplementary References

1 Y. Y. Liang, Y. G. Li, H. L. Wang, J. G. Zhou, J. Wang, T. Regier, H. J. Dai, *Nat. Mater.* 2011, *10* , 780-786.

2 Z. Y. Wu, X. X. Xu, B. C. Hu, H. W. Liang, Y. Lin, L. F. Chen, S. H. Yu, *Angew. Chem., Int. Edit.* 2015, *54* , 8179-8183.

3 Q. L. Zhu, W. Xia, T. Akita, R. Q. Zou, Q. Xu, *Adv. Mater.* 2016, *28*, 6391.

4 G. Li, X. L. Wang, J. Fu, J. D. Li, M. G. Park, Y. N. Zhang, G. Lui, Z. W. Chen, *Angew. Chem., Int. Edit.* 2016, *55*, 4977-4982.

5 Y. Hou, Z. H. Wen, S. M. Cui, S. Q. Ci, S. Mao, J. H. Chen, *Adv. Funct. Mater.* 2015, *25*, 872-882.

6 B. Y. Xia, Y. Yan, N. Li, H. B. Wu, X. W. D. Lou, X. Wang, *Nat. Energy*, 2016, *1*, 15006.

7 G. A. Ferrero, K. Preuss, A. Marinovic, A. B. Jorge, N. Mansor, D. J. L. Brett, A. B. Fuertes, M. Sevilla, M. M. Titirici, *Acs Nano* 2016, *10*, 5922-5932.

8 L. Lin, Q. Zhu, A. W. Xu, *J. Am. Chem. Soc.* 2014, *136*, 11027-11033.

9 Y. Z. Chen, C. M. Wang, Z. Y. Wu, Y. J. Xiong, Q. Xu, S. H. Yu, H. L. Jiang, *Adv. Mater.* 2015, *27*, 5010-5016.

10 W. Xia, R. Zou, L. An, D. Xia, S. Guo, *Energy Environ. Sci.* 2015, *8*, 568-576.

11 Z. H. Li, M. F. Shao, L. Zhou, Q. H. Yang, C. Zhang, M. Wei, D. G. Evans, X. Duan, *Nano Energy*, 2016, *25*, 100-109.

12 Z. S. Wu, L. Chen, J. Z. Liu, K. Parvez, H. W. Liang, J. Shu, H. Sachdev, R. Graf, X. L. Feng, K. Mullen, *Adv. Mater.* 2014, *26*, 1450-1455.

13 L. Shang, H. J. Yu, X. Huang, T. Bian, R. Shi, Y. F. Zhao, G. I. N. Waterhouse, L. Z. Wu, C. H. Tung, T. R. Zhang, *Adv. Mater.* 2016, *28*, 1668-1674.

14 S. Mao, Z. H. Wen, T. Z. Huang, Y. Hou, J. H. Chen, *Energy Environ. Sci.* 2014, *7*, 609-616.

15 X. Zhong, Y. Jiang, X. Chen, L. Wang, G. L. Zhuang, X. Li, J. G. Wang, *J. Mater. Chem. A*, DOI: 10.1039/C6TA03820D.

16 T. Ling, D. Y. Yan, Y. Jiao, H. Wang, Y. Zheng, X. L. Zheng, J. Mao, X. W. Du, Z. P. Hu, M. Jaroniec, S. Z. Qiao, *Nat. Commun.*, DOI:http://dx.doi.org.libproxy1.nus.edu.sg/10.1038/ncomms12876

17 N. Jiang, B. You, M. L. Sheng, Y. J. Sun, *Angew. Chem., Int. Edit.* 2015, *54*, 6251-6254.

18 J. F. Chang, Y. Xiao, M. L. Xiao, J. J. Ge, C. P. Liu, W. Xing, *ACS Catal.* 2015, *5*, 6874-6878.

19 H. F. Liang, F. Meng, M. Caban-Acevedo, L. S. Li, A. Forticaux, L. C. Xiu, Z. C. Wang, S. Jin, *Nano lett.* 2015, *15*, 1421-1427.

20 J. Masa, W. Xia, I. Sinev, A. Q. Zhao, Z. Y. Sun, S. Grutzke, P. Weide, M. Muhler, W. Schuhmann, *Angew. Chem., Int. Edit.* 2014, *53*, 8508-8512.

21 M. R. Gao, X. Cao, Q. Gao, Y. F. Xu, Y. R. Zheng, J. Jiang, S. H. Yu, *Acs Nano* 2014, *8*, 3970-3978.

22 Y. H. Su, Y. H. Zhu, H. L. Jiang, J. H. Shen, X. L. Yang, W. J. Zou, J. D. Chen, C. Z. Li, *Nanoscale*, 2014, *6*, 15080-15089.

23 C. Z. Zhu, D. Wen, S. Leubner, M. Oschatz, W. Liu, M. Holzschuh, F. Simon, S. Kaskel, A. Eychmuller, *Chem.Commun.* 2015, *51*, 7851-7854.

24 L. H. Wu, Q. Li, C. H. Wu, H. Y. Zhu, A. Mendoza-Garcia, B. Shen, J. H. Guo, S. H. Sun, *J. Am. Chem. Soc.* 2015, *137*, 7071-7074.

25 J. Masa, P. Weide, D. Peeters, I. Sinev, W. Xia, Z. Y. Sun, C. Somsen, M. Muhler, W. Schuhmann, *Adv. Energy Mater.*, DOI: 10.1002/aenm.201502313.

26 M. R. Gao, Y. F. Xu, J. Jiang, Y. R. Zheng, S. H. Yu, *J. Am. Chem. Soc.* 2012, *134*, 2930-2933.

27 S. Dou, L. Tao, J. Huo, S. Y. Wang, L. M. Dai, *Energy Environ. Sci.* 2016, *9*, 1320-1326.

28 A. Aijaz, J. Masa, C. Rosler, W. Xia, P. Weide, A. J. R. Botz, R. A. Fischer, W. Schuhmann, M. Muhler, *Angew. Chem., Int. Edit.* 2016, *55*, 4087-4091.

29 X. Liu, M. Park, M. G. Kim, S. Gupta, X. J. Wang, G. Wu, J. Cho, *Nano Energy*, 2016, *20*, 315-325.

30 Y. Liu, H. Jiang, Y. Zhu, X. Yang, C. Li, *J. Mater. Chem. A* 2016, *4*, 1694-1701.

31 H. B. Yang, J. W. Miao, S. F. Hung, J. Z. Chen, H. B. Tao, X. Z. Wang, L. P. Zhang, R. Chen, J. J. Gao, H. M. Chen, L. M. Dai, B. Liu, *Sci. Adv.*, DOI: http://dx.doi.org/10.1126/sciadv.1501122.

32 Z. Q. Jiang, Z. J. Jiang, T. Maiyalagan, A. Manthiram, *J. Mater. Chem. A* 2016, *4*, 5877-5889.

33 P. Ganesan, M. Prabu, J. Sanetuntikul, S. Shanmugam, *Acs Catal.* 2015, *5*, 3625-3637.

34 T. Y. Ma, S. Dai, M. Jaroniec, S. Z. Qiao, *J. Am. Chem. Soc.*, 2014, *136*, 13925-13931.